

# Scintillation Index of the Gaussian Beams Propagated through the Paths with Strong Turbulence

T. I. Arsenyan, N. A. Suhareva, A. P. Sukhorukov<sup>†</sup>, and A. A. Chugunov

*Department of Physics, Moscow State University, Moscow, 119991 Russia*

*e-mail: suhareva@phys.msu.ru*

Received January 12, 2014; in final form, March 31, 2014

**Abstract**—Theoretical and experimental studies of the local statistical characteristics of Gaussian beams propagated through the paths with strong turbulence were carried out and their results are presented. It is ascertained that the applicability of the scintillation index meanings are substantially limited for the assessment of the performance quality of the optical data transmitting channels. On the basis of the experimental data got under different propagation conditions the peculiarities of the localized intensity distributions and those of the scintillation index are revealed.

**Keywords:** open optical channel, scintillation index, laser beam, turbulence.

**DOI:** 10.3103/S002713491404002X

## INTRODUCTION

The development of modern open optical data-transmission channels was accelerated after the integration of space–time code structures and low-density methods for anti-noise coding of transmitted data streams. However, the majority of the code structures are developed under the assumption that the interference series are relatively short. This condition is often violated in a regime of high modulation rates and sub-channel multiplexing.

Turbulent disturbances of the medium remain a significant factor that limits the capacity of open optical channels. These disturbances evolve into strong disturbances state if the channel is several kilometers long (or is even longer). The lack of rigorous mathematical algorithms for fluctuations prediction under strong turbulence conditions results in excess reservation of the channel resources, increases the data unit processing time, and reduces the energy efficiency of the transceiver system.

The scintillation index is a commonly used parameter that characterizes the instability of open optical channels. This index was first used in astronomical observations and characterizes the relative fluctuations of intensity under narrow-angle signal reception [1]. Detailed experimental studies of the local profile of the scintillation index measured in the signal beam coverage area revealed the strong dependence of this parameter on the position and profile of the control aperture. We present a consistent description of the results that were obtained in our experiments with real

and model paths that were partially described earlier [2, 3].

## 1. A MULTI-GAUSSIAN BEAM IN A TURBULENT MEDIUM

Let us analyze the general case of propagation of a beam formed by several Gaussian components in a turbulent atmosphere. The practical relevance of this problem stems from the fact that modern multichannel optical systems may operate at bit rates in excess of 10 Gbit/s. Beams with complex spatial profiles allow one not only to use efficiently the space–frequency coding methods, but also to reduce significantly the energy losses which are inevitable when one works with wide high-power beams [4]. The Gaussian beam profile may be used as a basis for the formation of various spatial structures (a complex beam may be considered as a superposition of several Gaussian ones). For example, a cosh-Gaussian beam may be obtained by superposition of four decentered Gaussian beams with equal widths [5].

Let a multi-Gaussian beam with sources that have matching frequencies and are coherent and located in the same plane propagate along the  $z$  axis that is perpendicular to the plane of the sources (a similar approach was used in [6]). The beam disturbance corresponding to the beam at points with  $z = 0$  in the sources plane is as follows:

$$u(x, y, 0) = \sum_i^N u_i(x, y, 0), \quad (1)$$

where  $u_i(x, y, 0)$  is the  $i$ th Gaussian component.

<sup>†</sup> Deceased.

We define the width  $\omega_0$  and the coordinate of the radiator center  $(a_i, b_i, 0)$  for each Gaussian component of a unit amplitude:

$$u_i(x, y, 0) = \exp\left[-\frac{(x-a_i)^2 + (y-b_i)^2}{\omega_0^2}\right]. \quad (2)$$

Using the extended Huygens–Fresnel principle [7], we signify the average intensity in the receiver plane located at a distance  $z = L$  from the radiator in the following way:

$$\begin{aligned} \langle I(p, q, L) \rangle &= \frac{k^2}{(2\pi L)^2} \int_{-\infty}^{\infty} \int_{-\infty}^{\infty} \int_{-\infty}^{\infty} \int_{-\infty}^{\infty} u(x, y, 0) u^*(\xi, \eta, 0) \\ &\times \exp\left\{\frac{ik}{2L}[(p-x)^2 + (q-y)^2 - (p-\xi)^2 - (p-\eta)^2]\right\}^{(3)} \\ &\times \langle \exp[\psi(x, y, p, q) + \psi^*(\xi, \eta, p, q)] \rangle dx dy d\xi d\eta, \end{aligned}$$

where  $k = 2\pi/\lambda$  is the wavenumber,  $\lambda$  is the wavelength, and  $(p, q)$  are the transverse coordinates in the receiver plane. Angle brackets denote the ensemble average.

If we use the Kolmogorov–Obukhov model, the frozen turbulence approximation, and the structure function in the Rytov form [8], the ensemble averaged exponent of the difference of random phase incursions may be presented in the following form:

$$\begin{aligned} \langle \exp[\psi(x, y, p, q) + \psi^*(\xi, \eta, p, q)] \rangle &= \exp(-D_w/2) \\ &= \exp-[(x-\xi)^2 + (y-\eta)^2]^{5/6} / \rho_0^{5/3}, \end{aligned} \quad (4)$$

where  $D_w$  is the wave structure function for a spherical wave,  $\psi(x, y, p, q)$  is the random component of the complex phase of a spherical wave propagating from the source point to the receiver point, and  $\rho_0$  is the coherence length of a spherical wave. In the case under study,  $\rho_0$  takes on the following form:

$$\rho_0 = (0.545 \overline{C_n^2} k^2 L)^{-3/5},$$

where  $\overline{C_n^2}$  defines the average structure characteristic [10].

Let us define the partial coherence and mutual coherence functions for each pair of components of a multi-Gaussian beam [10]. Using the denotations introduced earlier in (1)–(3), one may write:

$$\begin{aligned} \Gamma_{ij}^{1,1}(p, q, L) &= \frac{k^2}{(2\pi L)^2} \int_{-\infty}^{\infty} \int_{-\infty}^{\infty} \int_{-\infty}^{\infty} \int_{-\infty}^{\infty} u_i(x_i, y_i, 0) u_j^*(x_j, y_j, 0) \\ &\times \exp\left\{\frac{ik}{2L}[(p-x_i)^2 + (q-y_i)^2 - (p-x_j)^2 - (p-y_j)^2]\right\} \\ &\times \langle \exp[\psi(x_i, y_i, p, q) + \psi^*(x_j, y_j, p, q)] \rangle dx_i dy_i dx_j dy_j. \end{aligned} \quad (5)$$

The average intensity of the multi-Gaussian beam in the receiving plane may be expressed as a sum of the partial functions of second-order coherence in the following way:

$$\langle I(p, q, L) \rangle = \sum_{i=1}^N \sum_{j=1}^N \Gamma_{ij}^{1,1}(p, q, L). \quad (6)$$

We define the radius of the multi-Gaussian beam component at an arbitrary distance from the sources plane in the additive approximation:

$$\omega = \omega_0(1 + \tau_1 + \tau_2)^{1/2}, \quad (7)$$

where  $\tau_1 = 4L^2/(k^2\omega_0^4)$  and  $\tau_2 = 8L^2/(k^2\omega_0^2\rho_0^2)$ . It may be assumed roughly that  $\tau_1$  characterizes the intrinsic diffraction spreading of the beam and  $\tau_2$  describes the beam distortion under turbulent conditions.

Having performed integration in the right part of Eq. (5) with account for the additive representation (7), one obtains the following:

$$\begin{aligned} \Gamma_{ij}^{1,1}(p, q, L) &= \frac{\omega_0^2}{\omega^2} \\ &\times \exp\left\{-\frac{2}{\omega^2}\left[\left(p - \frac{a_i + a_j}{2}\right)^2 + \left(q - \frac{b_i + b_j}{2}\right)^2\right]\right\} \\ &\times \exp\left\{\frac{ik\omega_0^2\tau_1}{2\omega^2 L}[(a_i - a_j)(a_i + a_j - 2p) \right. \\ &\quad \left. + (b_i - b_j)(b_i + b_j - 2q)]\right\} \\ &\times \exp\left\{-\frac{\tau_2}{2\omega^2}[(a_i - a_j)^2(b_i - b_j)^2] \right. \\ &\quad \left. + \frac{2}{\omega^2}\left[\left(\frac{a_i - a_j}{2}\right)^2 + \left(\frac{b_i - b_j}{2}\right)^2\right]\right\}. \end{aligned} \quad (8)$$

The technique of fractional powers substitution with integer values proposed in [12] was used in the integration and in the derivation of Eq. (8).

## 2. INTENSITY PROFILES AND SCINTILLATION INDEX OF GAUSSIAN BEAMS AT THE REAL PATH

The ensemble average of the multi-Gaussian beam intensity may be presented as follows:

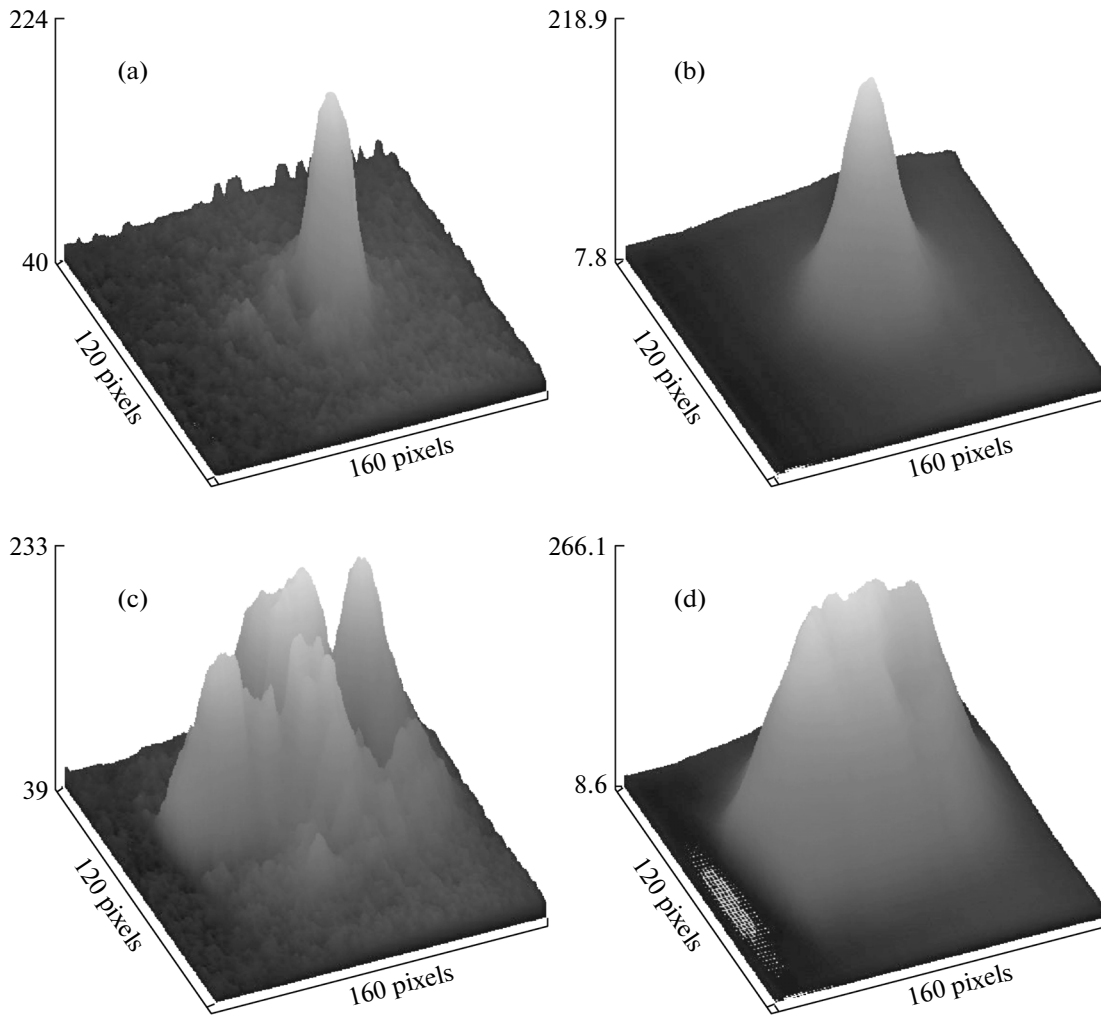


**Fig. 1.** The instantaneous (left) and ensemble averaged (right) distributions of the intensity in the beam-detection plane for the real path. The radius  $\omega_0$  is equal to 1.75 cm (upper) or 5 cm (bottom pictures).

$$\begin{aligned} \langle I(p, q, L) \rangle &= \sum_{i=1}^N \Gamma_{ii}^{1,1}(p, q, L) \\ &+ \sum_{i=1}^N \sum_{j=i+1}^N \text{Re}[\Gamma_{ij}^{1,1}(p, q, L)]. \end{aligned} \quad (9)$$

The contributions of individual components are separated here from the “superposition” contributions, whose stationarity is determined by both the spatial and the temporal coherence of basis beams. Let  $N = 1$  and  $a_1 = b_1 = 0$ . Then the average intensity of a solitary component is equal to the following:

$$\langle I(p, q, L) \rangle = \frac{\omega_0^2}{\omega^2} \exp\left[-\frac{2(p^2 + q^2)}{\omega^2}\right], \quad (10)$$

where the beam width is defined by Eq. (7). The above representation agrees with the results that were obtained earlier in [13].

The typical profiles of instantaneous and averaged intensity distributions of the intensity of the solitary Gaussian beams obtained at the real path are shown in Fig. 1. The upper pictures present the typical instantaneous profile and the result of averaging over 1000 counts for a beam with an initial radius of 1.75 cm, the lower ones correspond to a beam with an initial radius of 5 cm; the location path in one direction had the length of 300 m and the radiation wavelength was 0.628  $\mu\text{m}$ . Strong disturbances in the instantaneous intensity distributions of a beam with an initial radius of 5 cm and anisotropy and a truncated peak of the corresponding averaged distribution should be noted.

Let us discuss the case of a binary Gaussian beam comprised by components having equal initial widths and located symmetrically with respect to the origin of coordinates in the plane of the sources ( $a_1 = a_2 = 0$  and

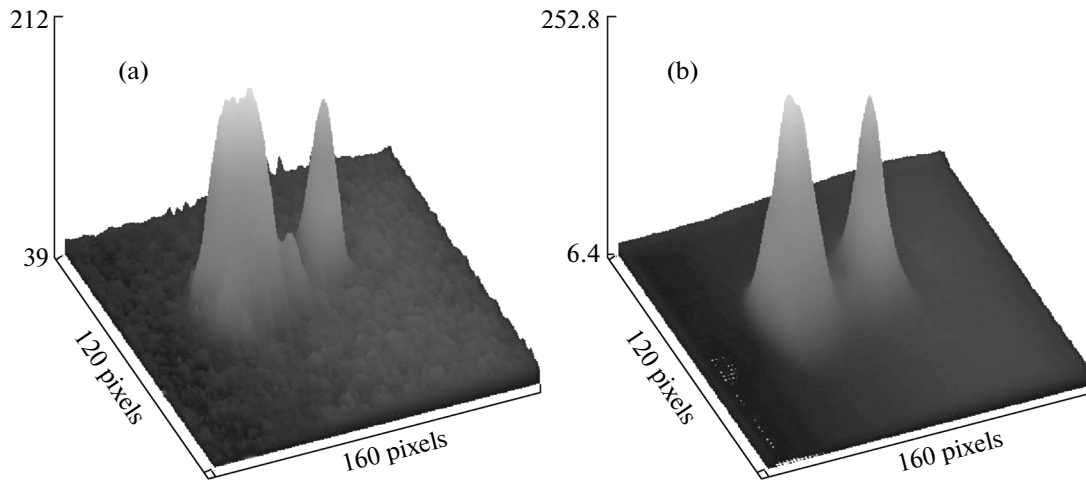


**Fig. 2.** The instantaneous (left) and ensemble averaged (right) distributions of the intensity of a binary Gaussian beam in the detection plane at the real path.

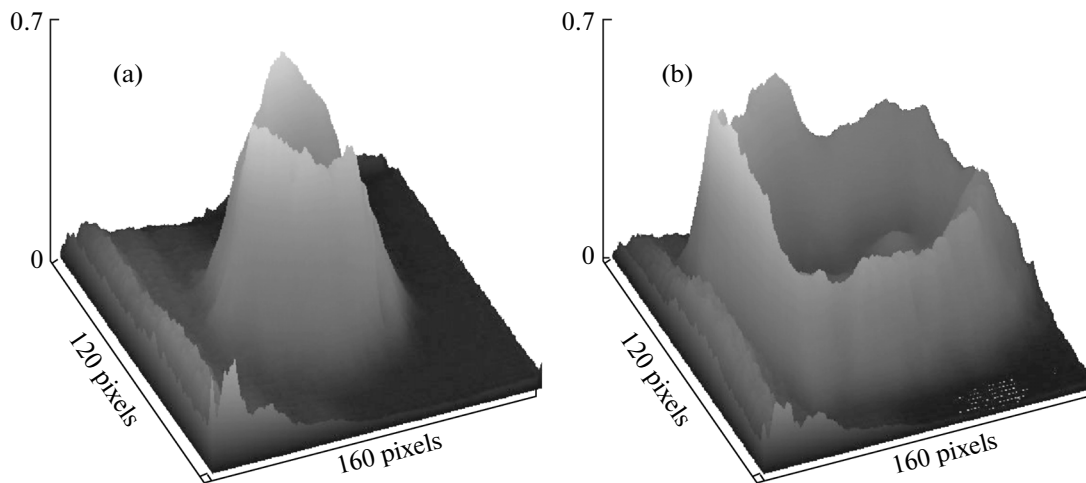


**Fig. 3.** The profiles of the local scintillation indices for the solitary Gaussian beams with (a)  $\omega_0 = 1.75$  cm or (b)  $\omega_0 = 5$  cm.

$b_1 = -b_2 = b$ ). The average intensity corresponding to the binary beam takes on the following form:

$$\begin{aligned} \langle I(p, q, L) \rangle &= \frac{\omega_0^2}{\omega^2} \exp\left\{ -\frac{2[p^2 + (q+b)^2]}{\omega^2} \right\} \\ &\times \left\{ 1 + \exp\left(\frac{8b}{\omega^2}q\right) + 2 \exp\left[\frac{2b}{\omega^2}(2q - b\tau_2)\right] \right. \\ &\left. \times \cos\left[\frac{2bk\tau_1\omega_0^2}{\omega^2 L}q\right] \right\}. \end{aligned} \quad (11)$$

The instantaneous binary beam profile and its profile averaged over the sample of 2000 counts for the case of splitting the initial beam into two components with different radii are shown in Fig. 2. The obtained com-

ponents exhibit initially high degrees of spatial and temporal coherence.

The interference spike observed in the left-side pictures of Fig. 2 between the initial positions of the Gaussian components may be attributed either to the retention of a high degree of mutual coherence of partial beams or to aberration distortions. A 2.4-fold difference in the radii of partial beams (0.5 and 1.2 cm respectively) was introduced initially into the experiment in order to simplify the monitoring of the binary beam components.

Detailed analysis shows that the averaged intensity profiles measured at the output of the real path differ from the initial Gaussian distributions (primarily in the region of high intensities). The distribution peak is pointed (cleaved) and has a discontinuous derivative practically in all cases considered. The distribution anomalies are even more pronounced in the profile of

the local scintillation indices (Fig. 3). The local scintillation index is hereinafter understood as that being calculated in the limit of a single pixel of the detected image. The spatial distribution of the scintillation index for beams of all the studied radii has a sharp and well-marked peripheral value area and nonsmoothable lower-level fluctuations in the paraxial regions. Such behavior of the second intensity moment is typical for fractal structures that develop in the regions of strong turbulent disturbances of the beam.

We express the scintillation index

$$\sigma_I^2(\mathbf{r}, L) = \frac{\langle I^2(\mathbf{r}, L) \rangle}{\langle I(\mathbf{r}, L) \rangle^2} - 1 \quad (12)$$

in terms of the second-order and fourth-order coherence functions. The partial function of fourth-order mutual coherence for a multicomponent beam at a distance  $L$  from the source plane is usually written as follows:

$$\begin{aligned} \Gamma_{ijnm}^{2,2}(\mathbf{r}, L) &= u_i(\mathbf{r}_1, L)u_j^*(\mathbf{r}_2, L)u_n(\mathbf{r}_3, L)u_m^*(\mathbf{r}_4, L) \\ &\times \langle \exp[\psi(\mathbf{r}_1, \mathbf{r}, L) + \psi^*(\mathbf{r}_2, \mathbf{r}, L) \\ &+ \psi(\mathbf{r}_3, \mathbf{r}, L) + \psi^*(\mathbf{r}_4, \mathbf{r}, L)] \rangle \end{aligned} \quad (13)$$

When a solitary beam is analyzed, the fourth-order coherence function (13) corresponds to the second moment of the intensity distribution in the detection plane and may be expressed in terms of the second-order coherence functions and the ensemble average of phase fluctuations in the second and third Born approximations [10]:

$$\begin{aligned} \langle I^2(\mathbf{r}, L) \rangle &= \Gamma^{2,2}(\mathbf{r}, L) = \langle I^2(\mathbf{r}, L) \rangle \\ &\times \exp\{2\text{Re}[E_2(\mathbf{r}_1, \mathbf{r}) + E_3(\mathbf{r}_1, \mathbf{r})]\}, \end{aligned} \quad (14)$$

where  $\text{Re}$  defines the real part of the argument and  $E_2$  and  $E_3$  are the second-order statistical moments of phase fluctuations. These moments are defined in the following way:

$$\begin{aligned} E_2(\mathbf{r}_1, \mathbf{r}) &= \langle \psi(\mathbf{r}_1, \mathbf{r}, L)\psi^*(\mathbf{r}_1, \mathbf{r}, L) \rangle, \\ E_3(\mathbf{r}_1, \mathbf{r}) &= \langle \psi(\mathbf{r}_1, \mathbf{r}, L)\psi(\mathbf{r}_1, \mathbf{r}, L) \rangle. \end{aligned} \quad (15)$$

The scintillation index may be roughly split into the longitudinal and transverse components:

$$\sigma_I^2(\mathbf{r}, L) = \sigma_{I,r}^2(\mathbf{r}, L) + \sigma_{I,L}^2(\mathbf{0}, L). \quad (16)$$

The scintillation index splitting into the longitudinal and transverse (relative to the beam propagation direction) components was carried out only to facilitate the discussion of the experimental characteristics. Such splitting for the Gaussian beams and different models of turbulent media was analyzed in detail in [9]. For example, the transverse scintillation index

component for the Kolmogorov turbulent atmosphere may be approximated in the following way:

$$\sigma_{I,r}^2(\mathbf{r}, L) \sim \frac{r^2}{\omega^2}, \quad (17)$$

where  $\omega$  is the effective partial beam radius at a distance  $L$  from the source.

The quadratic dependences of the transverse component of the scintillation index for a solitary Gaussian beam were predicted for all the applied turbulent atmosphere models (the Kolmogorov and von Karman models and the extended Andrews model) both for weak and strong turbulence conditions. They do not agree with the sharp peripheral increases in the fluctuation intensity observed over the real path. A summary table detailing the scintillation index dependence on the medium parameters and the path structure is found in [10].

### 3. THE INTENSITY AND SCINTILLATION INDEX PROFILES FOR A SOLITARY BEAM AT A MODEL PATH

Spatial distributions of the intensity and the scintillation index in the far-field zone for the beam propagating through a medium with variable turbulent disturbances were studied for thermally nonstationary media. This mode of turbulent flow development has a high degree of repeatability and, in contrast to the turbulence excitation under wind load, does not produce parasitic flows outside the model path region.

A series of experiments was performed at a model horizontal path with a heating element underneath it. The channel length is defined by the tilt angles of "driving" flat mirrors and equals to 7 m. At the model path the conditions of strong turbulence were provided. The operating region is enclosed in a cylindrical tube with a diameter of 0.2 m and has slit windows at the ends in order to eliminate the uncontrolled temperature and aerodynamic influences. A solid-state second-harmonic laser radiated a Gaussian beam at a wavelength of 0.48  $\mu\text{m}$  with a radius of 0.5 cm.

The intensity distributions dynamics at the path output were recorded with a PULNiX-1300 high-speed camera that allows one to capture video at a frame rate of 400 Hz (and higher frame rates) and a working field resolution of  $320 \times 240$  pixels and 10-bit intensity coding without additional compression and filtering. The individual sample length was no less than 20 s, the discretization interval was 2.5  $\mu\text{s}$  (i.e., each sample contained 8000 frames), and the working frame size was  $320 \times 240$  pixels at 8-bit digitization of local intensity.

At the initial stage of the experiments at a model path the authors of [11] evaluated the statistical characteristics of beam fluctuations under similar experimental conditions. The structural characteristics cor-

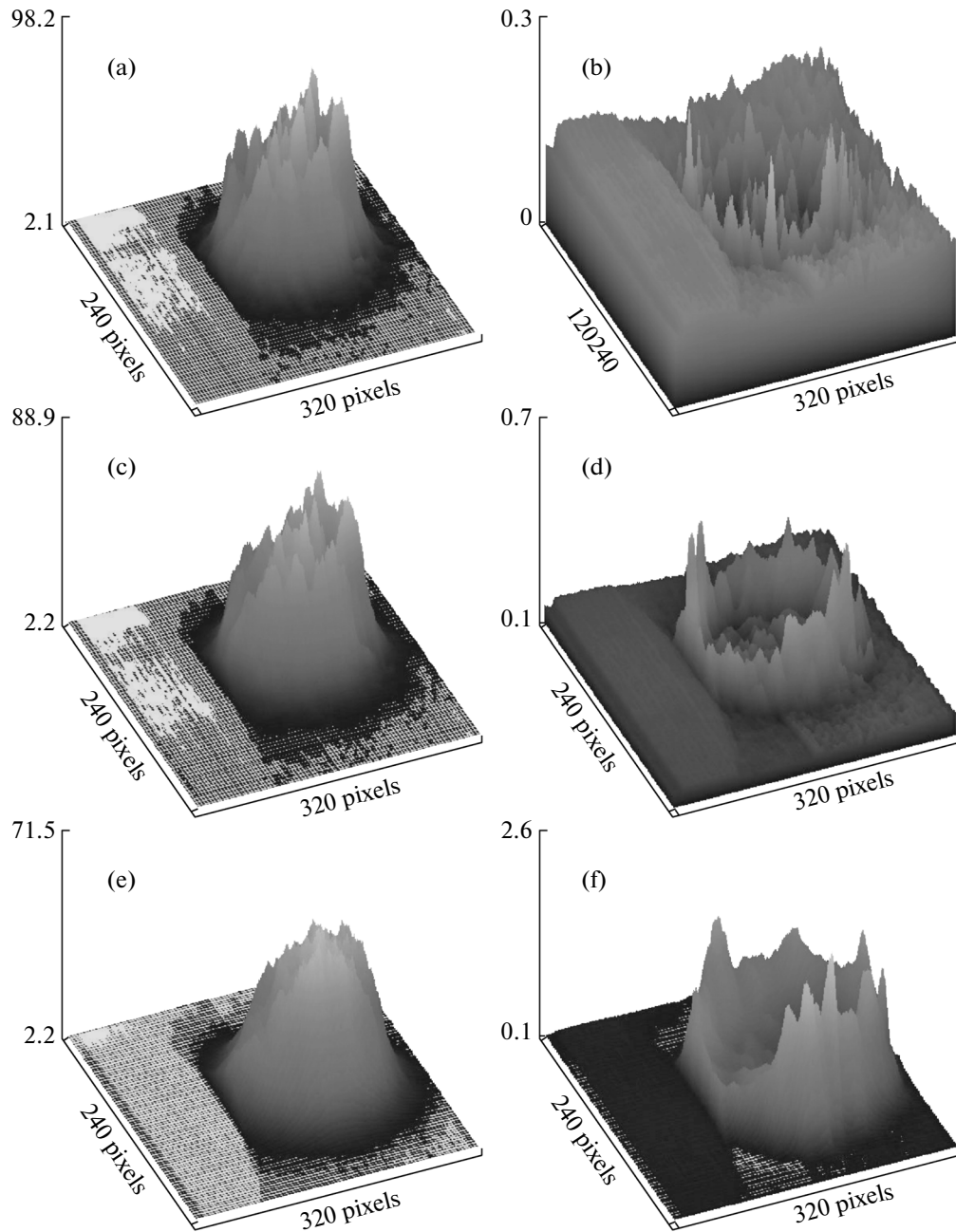


**Fig. 4.** The profiles of the average intensity distributions (a, c, e) and those of the scintillation index (b, d, f) for various temperature gradients (500, 700, and 1500 deg/m).

responding to various degrees of the strong turbulence development were calculated based on these evaluations. The values of the structural characteristics under the conditions at the model path are of the following order of magnitude:

(i)  $C_n^2 \sim 10^{-10} \text{ cm}^{-2/3}$  if the temperature gradient value is lower than 350 deg/m,

(ii)  $C_n^2 \sim 10^{-9} \text{ cm}^{-2/3}$  if the temperature gradient value spans from 500 to 750 deg/m, and

(iii)  $C_n^2 \sim 10^{-8} \text{ cm}^{-2/3}$  if the temperature gradient value is higher than 1000 deg/m.

Only the temperature gradient values are indicated hereinafter in the descriptions of detection conditions.

The sequence of the intensity distribution frames was analyzed as a statistical ensemble, and the first and the second moments of the intensity distribution function were calculated for each pixel of this ensemble. Such values in fact correspond to a transition to extremely low aperture values. Figure 4 shows the pro-

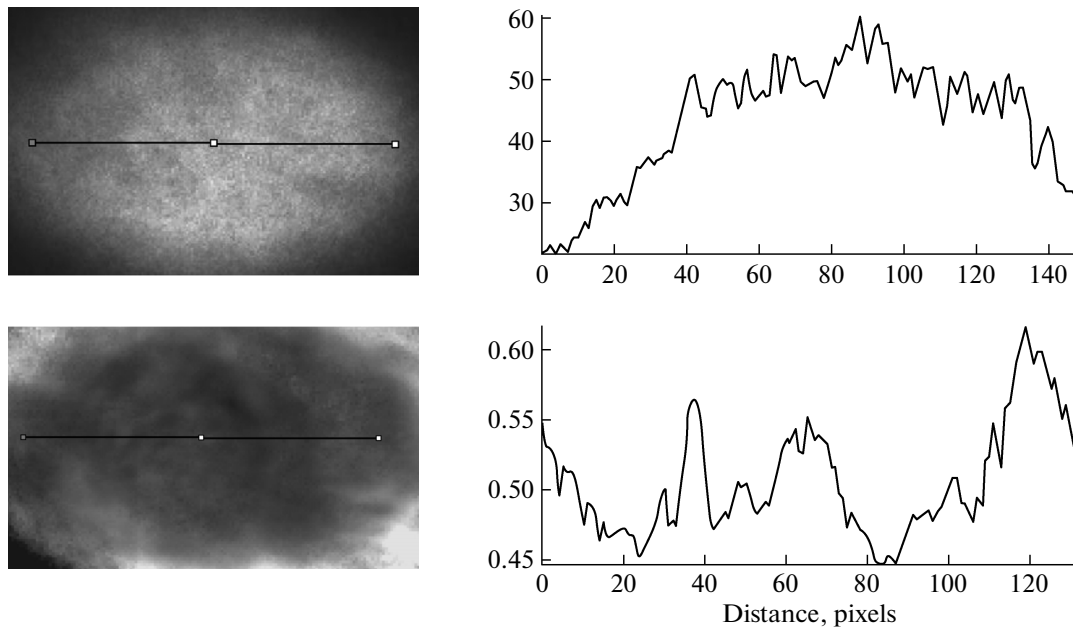


**Fig. 5.** The intensity (upper) and scintillation index (bottom) averaged over an ensemble of 8000 frames and the corresponding central vertical sections.

files of intensity and the scintillation index for three modes of the model surface heating (i.e., for a temperature gradient of 500 deg/m (upper), 750 deg/m (middle), or 1500 deg/m (bottom pictures)). The high peripheral level of the scintillation index in Fig. 4b corresponds to fluctuations of the background signal of the detecting matrix. The almost complete lack of background in the distribution profiles on the left may be attributed to the procedure of exclusion of the minimum background value at shaded periphery.

The high degree of spatial inhomogeneity of the first and second moments should be noted. This implies that they are practically inapplicable for the estimation of the performance quality of an open optical data-transmission channel under the conditions of strong turbulence. The presented scintillation index profiles feature a well-marked “crown” of high fluctuation levels. The observed crown differs substantially in its height (with respect to the central part), “steepness,” and “width” from the described in [14] effect of an increase in scintillation index in the region of high intensity gradient. The formation of a well-marked crown for the Gaussian beam profile under the studied experimental conditions may be associated with the divergence of the corresponding correlation integrals. This divergence is characteristic for the formation of caustics [15] or for the fractal-type phase modulation.

The sections of the central parts of the intensity and scintillation index profiles (not including the crown region) shown in Fig. 5 confirm the earlier-stated hypothesis on the low informative value of the scintillation index values measured experimentally: the resulting value depends strongly on the detecting aper-

ture and its position relative to the center of the formed spot. The graphic fractal properties of the experimentally observed profiles of intensity and its second moment preclude the use of direct correlation methods in the studies of such distributions. In this context, the only adequate solution may be provided by the analysis of a statistical ensemble of the fractal intensity distributions with the use of the nonequilibrium statistics methods and the selection of macroscopic parameters that are adequate to the physical process and characterize the ensemble state unambiguously.

#### 4. PROFILES OF THE INTENSITY DISTRIBUTIONS AND SCINTILLATION INDEX OF DIFRACTALS

Diffractals are defined as waves that propagated through or were reflected from a fractal structure [16]. The interaction with a fractal structure leaves an imprint on the amplitude or phase modulation of the initial wave in the entire range of feasible scales. The peculiarities of diffractal modulation completely preclude the use of the geometric optics approximations at any scales of the propagation problems analysis. The diffractal regime is often treated as a special one (i.e., wavefront-surface “discontinuities” are allowed) in the propagation or scattering problems.

In order to exclude edge effects, the wavefront curvature of the incident wave, and the influence of the amplitude modulation of the initial beam, let us analyze the propagation of a plane wave through a phase-modulating screen with one-dimensional fractal spatial modulation of the optical density  $h(x)$ . A wave

propagating along the  $z$  direction is set in the following way:

$$u(x, z) = e^{ikz} (z < 0). \quad (18)$$

A wave that passed through the phase screen one can write as follows:

$$u(x, 0^+) = e^{ikh(x) + i\phi_0}. \quad (19)$$

The wave propagates freely after the phase plate ( $z > 0$ ), and the corresponding function  $u(x, z)$  may be calculated using the standard diffraction theory methods. Accordingly, one may determine the second-order and fourth-order coherence functions of the propagated wave in the far diffraction zone, the first and second moments of the intensity distribution, and the scintillation index:

$$I(x, z) \equiv |u(x, z)|^2, \quad I_2(x, z) \equiv \langle |u(x, z)|^4 \rangle. \quad (20)$$

Let the modulation profile of the wavefront  $h(x)$  be a random Gaussian function of  $x$  at  $z = 0^+$  [17]. Such an assumption is needed to simplify the analytical transformations at the first stage of estimation of the intensity distribution moments and to apply the following relationships in the calculation of the linear functionals  $G$  of  $h(x)$ :

$$\langle e^{iG(h(x))} \rangle = e^{i\langle G \rangle} e^{-\langle G^2 \rangle - \langle G \rangle^2 / 2}. \quad (21)$$

The determination of  $\langle G \rangle$  and  $\langle G^2 \rangle$  typically requires the calculation of the values  $\langle h \rangle$  and the correlation  $\langle h(x_1)h(x_2) \rangle$ , but  $h(x)$  is treated here as a fractal function and has infinitely large values of correlation and covariation  $\langle h^2 \rangle$ .

We use the spatial spectrum  $\bar{H}(\phi)$  to describe  $h(x)$  and introduce the power model (typical of fractal functions) of approximation of the spatial spectral density:

$$\bar{H}(\phi) = T/|\phi|^\alpha \quad (1 < \alpha < 3), \quad (22)$$

where  $T$  is the topothesis,  $\alpha = 5 - 2D$ , and  $D$  is the fractal dimensionality of the  $h(x)$  function.

It follows from (22) that the autocorrelation function  $h(x)$  tied to the Fourier transform  $\bar{H}(\phi)$  by the Wiener–Khinchin relation (particularly,  $\langle h^2 \rangle$ ) is in the general case infinite by virtue of the power approximation of the spectral density. However, the statistical properties of field fluctuations of diffractal structures may be determined from a series of variational integral parameters. Using Eq. (21), we obtain the following

formula for the mean-square value of the wave phase variation at the phase screen output:

$$\begin{aligned} \langle (h(x + \varepsilon) - h(x))^2 \rangle &= \int_{-\infty}^{\infty} d\phi \bar{H}(\phi) (e^{i\phi\varepsilon} - 1) \\ &= \frac{2T}{\alpha - 1} \sin \frac{\pi}{2} (2 - \alpha) \Gamma(2 - \alpha) |\varepsilon|^{\alpha - 1}. \end{aligned} \quad (23)$$

The properties of the fractal function topothesis [18] dictate that the following condition should be satisfied:

$$\langle (h(x + T) - h(x))^2 \rangle / T^2 \equiv 1. \quad (24)$$

The following relationship, which will be used later in the calculation of the second-order and fourth-order coherence functions for the studied diffractals, is valid at relatively low values of the argument of the trigonometric function in (23):

$$\langle (h(x + \varepsilon) - h(x))^2 \rangle = T^{2(D-1)} |\varepsilon|^{4-2D}. \quad (25)$$

The problem of propagation of a wave with phase-fractal modulation is characterized by the formal simplicity of statement. But it does not have a simple continuation in the standard form of the application of the Huygens–Fresnel principle and the calculation of a spatial Fourier transform. The split wavefront makes the integrals divergent may be “patched partially” with the use of a paraxial approximation. This approximation is valid in a limited range of the optical density variations gradient. Under such conditions the wave field beyond the modulating screen one can write as follows:

$$\begin{aligned} u(x, L) &= e^{i(kL - \pi/4)} \left( \frac{k}{2\pi L} \right)^{1/2} \\ &\times \int_{-\infty}^{\infty} \exp(ik[h(\xi) + (x - \xi)^2/2L]) d\xi, \end{aligned} \quad (26)$$

where  $L$  is the distance from the phase screen to the intensity distribution detection plane.

We obtain the second-order coherence function through integration:

$$\begin{aligned} \langle u(x, L) u^*(x + \varepsilon, L) \rangle &= \frac{k}{2\pi L} \\ &\times \int_{-\infty}^{\infty} \int_{-\infty}^{\infty} \langle \exp[h(x_1) - h(x_2)] \rangle \\ &\times e^{ik[(x-x_1)^2 - (x+\varepsilon-x_2)^2]/2L} dx_1 dx_2 \\ &= \exp \left[ \frac{-k^2 T^{2(D-1)} |\varepsilon|^{2(2-D)}}{2} \right]. \end{aligned} \quad (27)$$

The result of integration of (27) does not depend on the distance from the modulating screen and is  $\langle |\psi|^2 \rangle =$

$\langle I \rangle = 1$  at the axis. This agrees with the energy-conservation law.

The angular spectrum of the second-order coherence function may be obtained as a result of Fourier transformation of (27):

$$P_I(\phi) = \frac{1}{2\pi k} \int_{-\infty}^{\infty} \exp\left[-\frac{(kT)^{2(D-1)}|\varepsilon|^{2(2-D)}}{2}\right] e^{i\phi\varepsilon/k} d\varepsilon. \quad (28)$$

In the limits of small and large deviation angles the following approximations are valid [19]:

$$\begin{aligned} & kP_I(\phi) \\ \rightarrow & \begin{cases} \frac{2^{\frac{1}{2(2-D)}}\Gamma\left[1 + \frac{1}{2(2-D)}\right]}{\pi(kT)^{\frac{D-1}{2-D}}} & (|\phi| \rightarrow 0), \\ (kT)^{2(D-1)} \sin[\pi(2-D)]\Gamma\left[\frac{5-2(D)}{2\pi|\phi/k|^{5-2D}}\right] & (|\phi| \rightarrow \infty). \end{cases} \quad (29) \end{aligned}$$

Note that the obtained angular spectrum has a pointed peak in the direction of wave propagation. This was observed experimentally for the beams at the real and model paths. The shape of the dependence of the intensity fluctuation spectrum at small angles allows one to define the characteristic scale of the spatial frequency of diffracted waves:

$$Q = \left[\frac{2\pi T}{\lambda}\right]^{\frac{D-1}{2-D}}. \quad (30)$$

In order to determine the fourth-order coherence function with respect to the field or second-order coherence with respect to intensity, one has to calculate the ensemble averaged value of the separated phase incursions of the following form:

$$\begin{aligned} & \langle (h(x_1) + h(x_2) + h(x_3) + h(x_4))^2 \rangle \\ & = T^{2(D-1)} (|x_1 - x_3|^{4-2D} + |x_2 - x_4|^{4-2D} \\ & \quad + |x_2 - x_3|^{4-2D} + |x_1 - x_4|^{4-2D} \\ & \quad + |x_1 - x_2|^{4-2D} + |x_3 - x_4|^{4-2D}). \end{aligned} \quad (31)$$

This calculation is performed with the use of condition (21) that was formulated earlier and the relationships for the phase structure function of diffractal.

Let us introduce the following dimensionless parameter:

$$\zeta \equiv \frac{kL(kT)^{(D-1)/(2-D)}}{2^{1/(4-2D)}} = \frac{kLQ}{2^{1/(4-2D)}}. \quad (32)$$

When the ensemble averaged value of the phase incursion is inserted into the corresponding correla-

tion integral, we obtain the following expressions for the near and far regions of the diffractal propagation:

$$\begin{aligned} I_2^{near}(\zeta) &= 1 + \frac{2^{5-2D}}{\sqrt{\pi}} \zeta^{2-D} \Gamma\left[\frac{5-2D}{2}\right] \\ & \quad + O(\zeta^{4-2D}) \quad \zeta \rightarrow 0, \\ I_2^{far}(\zeta) &\rightarrow 2 - \frac{A(D)}{\zeta} \quad \zeta \rightarrow \infty, D > 1, 5. \end{aligned} \quad (33)$$

The  $A(D)$  factor, which is dependent on the fractal dimensionality of the modulating function, may be expressed analytically in certain exceptional cases (e.g., at  $D = 1.5$ ).

The fourth-order coherence function for the diffractal field has the following limiting values in the near and far regions:

$$I_2(\zeta) = \begin{cases} 1 & (\zeta \rightarrow 0), \\ 2 & (\zeta \rightarrow \infty). \end{cases} \quad (34)$$

The question of the monotonic nature of the fourth-order coherence function is of definite interest (primarily in the context of explaining the crown region observed in the spatial profile of the scintillation index). The intensity fluctuations maximum may be formed in the region of intermediate values of  $\zeta$  at  $D < 1.5$ . However, this mode should not be confused with the dynamic focusing processes as the fractal wavefront is not differentiable and thus does not have a normal.

The scintillation index in the discussed multifractal approximation equals to  $(I_2(\zeta) - 1)$ , is minimized in the paraxial region regardless of the distance from the phase screen to the detection plane, and is increased with increasing the deviation from the axis. The pattern of the scintillation index variations depends on the fractal dimensionality of the modulating function, the initial wavefront curvature, and the profile of amplitude modulation of the real beam.

Fractal descriptions of the physical properties of a medium have become widely used in problems of radiophysics and optics in the last decade. The interest in fractal and multifractal processes goes primarily from repeated experimental observations of the effect of “transfer” of the fractal dimensionality value for space–time structures of the inhomogeneous medium onto the fractal properties of the beam intensity fluctuations.

## CONCLUSIONS

The results of experimental studies of the localized spatial profiles of the first and second moments of the intensity distribution for the Gaussian beams at the real and model paths allow to conclude that it is not entirely correct to use the local value of the scintillation index and its value averaged over the arbitrarily

positioned apertures for estimating the quality of open optical data transmission channels.

The discrepancies in the descriptions of spatial distortions structure of Gaussian and multi-Gaussian beams under strong turbulence given by the traditional theoretical model that uses the concept of a continuous wavefront and the experimental results obtained for real and model optical paths may be resolved under the assumption that strong local modulation of the optical density results in a “discontinuity” of the wavefront.

The experimentally observed distinct spatial separation of the scintillation index profile detected on both the real and model paths into a high-level crown surrounding the exposure region and a crater within the region with nonsmoothable spatial modulations of the values is indicative of the development of a fractal or multifractal structure of the beam phase distortions in the process of propagation through a strongly turbulent medium [20]. The simplest model of difractal statistics confirms the presence of the observed features in the paraxial and peripheral beam regions.

The theoretical model discussed is limited by monofractal wavefront distortion. It is common practice to use multifractal models under the conditions of fully-developed turbulence. The methods described above may be used in these models only to obtain rough estimates of the fluctuation properties of the radiation field. The initial beam profile that is formed under nonstable generation modes is another significant source of the wavefront fractal distortions in open optical data transmission channels [21]. This source should be taken into account in the interpretation of the results.

The transfer of fractal and multifractal characteristics from the nonequilibrium-statistical properties of the propagation medium onto the space–time statistical characteristics of the propagating beam allows one to use nonextensive characteristics (such as the Rényi entropy and the Tsallis entropy) to describe fluctuation processes. This is a significant addition to the analytical ways of studies of the problems of radiation propagation in strongly nonequilibrium media.

#### ACKNOWLEDGMENTS

The present study was supported financially by the Russian Foundation for Basic Research (project no. 14-02-00461).

#### REFERENCES

1. L. C. Andrews, R. L. Phillips, and C. Y. Hopen, *Laser Beam Scintillation with Applications*, SPIE Press, (2001).
2. T. I. Arsenyan, M. I. Babanina, N. A. Suhareva, and A. P. Sukhorukov, *Zh. Radioelektr.*, No. 7, 4 (2013). <http://jre.cplire.ru/jre/jul13/8/text.html>
3. T. I. Arsenyan, N. A. Suhareva, and A. P. Sukhorukov, *Mos. Univ. Phys. Bull.* **69**, 55 (2014).
4. J. Wallace, I. Itzkan, and J. Camm, *J. Opt. Soc. Am. A* **64**, 1123 (1974).
5. Y. Zhang, Y. Song, Z. Chen, J. Ji, and Z. Shi, *Opt. Lett.* **32**, 292 (2007).
6. Xiusiang Chu, Zejin Liu, and Yi Wu, *J. Opt. Soc. Am. A* **25**, 74 (2008).
7. Yu. A. Kravtsov and Z. I. Feizulin, *Izv. Vyssh. Uchebn. Zaved., Khim. Khim. Tekhnol. Ser. Radiofiz.* **10**, 886 (1967).
8. S. M. Rytov, Yu. A. Kravtsov, and V. I. Tatarskii, in *Introduction to Statistical Radiophysics. Part 2*, (Moscow, 1978) [in Russian].
9. W. B. Miller, J. C. Ricklin, and L. C. Andrews, *J. Opt. Soc. Am. A* **11**, 2719 (1994).
10. L. C. Andrews and R. L. Phillips, *Laser Beam Propagation through Random Media* (SPIE Press, 2005).
11. T. I. Arsenyan, P. V. Korolenko, V. G. Lomonosov, and I. A. Tanacheev, *Radiotekhnika*, No. 1, 30 (2005).
12. H. T. Yura and S. G. Hanson, *J. Opt. Soc. Am. A* **4**, 1931 (1987).
13. H. T. Eyyuboglu and Y. Baykal, *Optics Express* **12**, 4659 (2004).
14. V. E. Zuev, V. A. Banakh, and V. V. Pokasov, *Optics of Turbulent Atmosphere* (Leningrad: Hydrometeoizdat, 1988) [in Russian].
15. Yu. A. Kravtsov and Yu. I. Orlov, *Geometrical Optics of Inhomogeneous Media* (Moscow: Nauka, 1980) [in Russian].
16. M. V. Berry, *J. Phys. A: Math. Gen.* **12**, 781 (1979).
17. S. O. Rice, *Bell. Syst. Tech. J.* **24**, 46 (1945).
18. M. V. Berry and J. H. Hannay, *Nature* **273**, 573 (1978).
19. M. V. Berry, *J. Phys. A: Math. Gen.* **10**, 2061 (1977).
20. T. I. Arsenyan, A. M. Zotov, P. V. Korolenko, M. S. Maganova, and I. A. Tanachev, *Opt. Atmos. Okeana* **19**, 1013 (2006).
21. M. V. Berry, *Optics Commun.* **200**, 321 (2001).

*Translated by D. Safin*